

1 Tracking Ionospheric Changes during Solar Eclipses: Concepción

2 Historical Data

3 Adán Y. Godoy¹, Manuel A. Bravo¹, Benjamín A. Urra¹, Carlos A. Castillo-Rivera^{2,3}, Marayén R.
4 Canales⁴, Alberto J. Foppiano¹

5 ¹Centro de Instrumentación Científica, Universidad Adventista de Chile, Chillán, Ñuble, Chile

6 ²Istituto Nazionale di Geofisica e Vulcanologia, Rome, Italy

7 ³Dipartimento di Ingegneria Civile, Edile e Ambientale, Sapienza Università di Roma, Roma, Italy

8 ⁴Departamento de Física, Universidad de Santiago de Chile, Estación Central, Santiago, Chile

9 *Correspondence to:* Manuel A. Bravo (manuelbravo@unach.cl)

10 Abstract.

11 Solar eclipses offer a unique natural experiment to probe ionospheric responses to sudden reductions in solar radiation. This
12 study reports the recovery of historical ionogram records to analyze the ionospheric response to solar eclipses spanning
13 several decades over Concepción (36.79°S, 73.03°W) / Chillán (36.64°S, 71.99°W). Out of 21 identified events between
14 1958 and 2024, data from 16 (76%) cases were rescued, many originally on fragile or hazardous 35 mm film, emphasizing
15 the scientific value of long-term datasets. Critical frequencies (foE, foF1, foF2) and virtual heights (h'E, h'F1, h'F/F2) were
16 extracted from digitized and scaled ionograms to quantify eclipse-induced perturbations. Diurnal variations show typical
17 dips in the E- and F1-layer critical frequencies, while F2-layer responses are more complex and variable. Regression analysis
18 was performed exclusively on critical frequencies, revealing a nearly linear decrease of foE and foF1 while the maximum
19 obscuration percentage of the eclipse is higher, whereas inconsistent behavior was observed on foF2. High-cadence
20 observations, available for select events, provided a significantly clearer depiction of the response to the eclipses than 1-hour
21 resolution historical data. Only the 2 July 2019 and 14 December 2020 eclipse responses had been previously published.
22 Predictions for the 06 February 2027 eclipse indicate an expected $\% \Delta \text{foE}$ decrease of $\sim 28\%$ and a $\% \Delta \text{foF1}$ decrease of $\sim 24\%$
23 at Chillán, offering a timely opportunity to validate the regression models and assess predictive skill.

24 1 Introduction

25 Solar eclipses offer unique opportunities to understand how the ionosphere reacts when solar radiation is interrupted during
26 daylight conditions. A "small night" generated by a total solar eclipse produces disturbances in the ionosphere, both directly
27 by the suppression of incident radiation or induced by chemical and transport processes. As solar radiation decreases, the
28 electron concentration of the ionospheric layers E and F1, which mainly depend on the production and loss terms, decrease
29 considerably or even disappear throughout the eclipse. Other layers, such as the F2 layer, for which the electron

30 concentration depends significantly on plasma transport by neutral winds and electrodynamics, react with delays and are
31 difficult to predict (Le et al., 2009; Hoque et al., 2016; Zhang et al., 2024). Furthermore, the ionosphere's response depends
32 on regional conditions and external factors such as space weather and lower atmospheric coupling. Additionally, changes in
33 the virtual and real heights of ionospheric layers, such as h'F1, h'F/F2, and hmF2, have been frequently reported, generally
34 showing an upward motion followed by a post-maximum descent as the ionosphere recovers (Le et al., 2008; Chuo, 2013 ;
35 Zhang et al., 2024).

36 Historically, from 1920 onward, studies of solar eclipses have progressively revealed how reduced solar radiation affects the
37 ionosphere and its coupled electrodynamic processes (Mitra et al., 1933; Ratcliffe, 1956; Rishbeth, 1968). Early radio
38 observations established solar radiation as the main ionization source and highlighted layer-specific density and plasma
39 transport effects (Higgs, 1942; Evans, 1965a, 1965b). These early eclipse experiments also contributed to the development of
40 ionospheric recombination theories and to the identification of characteristic temporal delays in ionospheric recovery
41 processes. From 1960–2015, hundreds of studies based on observations with instruments such as Very Low Frequency
42 (VLF) receivers, Global Navigation Satellite System (GNSS) arrays, ionosondes, riometers, incoherent scatter radars and
43 Doppler systems have determined eclipse-induced variations in Total Electron Content (TEC), critical frequency (foF2) and
44 height of the maximum electron density of the F2 layer (hmF2), electron temperature, and ion velocities (Cheng et al., 1992;
45 Afraimovich et al., 2002; Jakowski et al., 2008; Le et al., 2008; Momani et al., 2010; Kumar et al., 2013; Pezzopane et al.,
46 2015). These studies have consistently shown that during eclipses there are delayed responses, latitude-dependent effects,
47 and evidence of acoustic gravity waves (AGWs) and traveling ionospheric disturbances (TIDs) associated with eclipse
48 conditions (Cheng et al., 1992; Jakowski et al., 2008; Kumar et al., 2013). In several cases, eclipse-induced perturbations
49 were found to differ substantially between the E, F1, and F2 regions, reflecting the distinct chemical and dynamical
50 processes governing each ionospheric layer. Major events like the 2017 Great American Eclipse provided unprecedented
51 high-resolution data, allowing detailed modeling and confirmation of earlier findings (Huba & Drob, 2017; Reinisch et al.,
52 2018; Lei et al., 2018; Aryal et al., 2019), while recent studies emphasize the role of geomagnetic activity and AGW
53 generation in modulating post-eclipse ionospheric dynamics. Recent studies have also emphasized the importance of
54 combining long-term ionosonde records with modern GNSS observations to better characterize regional ionospheric
55 responses to eclipse forcing. A detailed review of these studies is compiled in Appendix A of Bravo et al. (2020).

56 Early days determination of ionospheric responses during solar eclipses were made mainly from ionosonde (vertically
57 incidence HF radar) observations. There are long time series of these observations, allowing the study of ionospheric long-
58 term trends. Early works are, for example, those of Smith and King (1981), Bremer (1992), Ortiz de Adler et al. (1997),
59 Jarvis et al. (1998), Foppiano et al. (1999). Later work has been reviewed by Lastovicka et al. (2017, and references therein)
60 and recent progress reported by Lastovicka (2023). One of these long-term series also offers a unique dataset to analyze both

61 short-term eclipse-induced ionospheric variations and broader temporal trends in the South American sector (Bravo et al.,
62 2020).

63 A vast historical record of ionograms is preserved on physical media, the recovery of which is essential for constructing
64 long-term time series. This information is key to conducting long-term trend studies that contribute to a better understanding
65 of the behavior and evolution of the regional ionosphere. Therefore, this work aims to demonstrate the scientific value of
66 rescuing this analog material by digitizing it and correctly extracting the relevant ionospheric parameters.

67 The purpose of this work is to characterize the response of the Concepción (36.79°S, 73.03°W) / Chillán (36.64°S, 71.99°W)
68 ionosphere under solar eclipse conditions, so that its response can be associated with parameters such as the maximum
69 obscuration level or time of day in order to predict the response for future eclipses.

70 **2 Methodology**

71 **2.1 Eclipse Event Selection and Station Characteristics**

72 A comprehensive search was conducted to identify all solar eclipse events whose trajectory passed over the ionospheric
73 observation stations in central Chile during the period 1957–2024.

74 Ionospheric characteristics during these events were selected from the long series of ionosonde records (ionogram) of
75 ionospheric station j3o: Concepción (36.79°S, 73.03°W). The Concepción ionosonde was a C4 type (1-25 MHz range) and
76 associated antennae (crossed deltas), installed in 1957 at the Universidad de Concepción, Andalien campus, by personnel
77 from the National Bureau of Standards (NBS, USA) for the International Geophysical Year (Ramírez, 1963). Later, the
78 ionosonde was moved to the nearby Bellavista campus (less than 2 km), the sweep range modified (0.25-20 MHz) and the
79 antennae improved to make better use of the quiet electromagnetic environment (adjustable folded dipole 0.25 to 3 MHz and
80 log-periodic 3 to 20 MHz). Maintenance difficulties of the antennae lead to a change during 1975 (cross deltas again). The
81 C4 ionosonde operated till 1994 with a transmitted power of approximately 1–5 kW, and employed simple pulse
82 transmissions without signal coding. Ionograms were recorded on 35 mm film. The interpretation and scaling required
83 optical projection on a screen and visual determination of parameters using a manual overlay. The j3o station resumed
84 operation in 1999. An IPS 42 type ionosonde (1- 22 MHz) was installed using the existing antennae. Recording was changed
85 from photographic to digital and routine observations were made until 2012, when it was relocated approximately 100 km
86 northeast to Chillán (36.64°S, 71.99°W), renamed as j3p, as part of an instrumentation modernization program (Ovalle et al.,
87 2017). For a short time interval a Canadian Advanced Digital Ionosonde (CADI) was also used. The ionosondes were
88 operated by dedicated academics, supported by electronic engineers and technicians (Muzzioli, 1977; Bravo et al., 2011),
89 providing continuous and high-quality measurements of ionospheric parameters (critical frequencies, virtual heights, etc.).
90 The ionosonde and antennae changes do not preclude standard accuracy of critical frequencies and virtual heights since these

91 parameters are not very system gain sensitive. Both locations share similar geomagnetic latitude characteristics, enabling the
92 construction of a long-term ionospheric database representative of the mid-latitude South American sector.

93 From the initial catalog of eclipse events identified, we selected those with solar obscuration exceeding 15% as observed
94 from the station coordinates (21 events). This threshold was established to ensure detectable ionospheric perturbations while
95 maintaining sufficient statistical samples for comparative analysis. Selected events span various phases of the solar cycle and
96 include eclipses with obscuration levels ranging from partial to near-totality, providing a diverse dataset for investigating the
97 relationship between eclipse magnitude and ionospheric response.

98 **2.2 Historical Ionogram Database**

99 Ionospheric observations analyzed in this study comprise a unique historical archive of vertical incidence ionograms
100 recorded between 1958 and 2024. The sounding cadence varied throughout the operational period, with temporal resolutions
101 of 1 hour, 30 minutes, 15 minutes, 5 minutes and 1 minute, depending on scientific objectives and operational constraints of
102 each campaign period. Higher-cadence observations (1–5 minute intervals) were typically implemented during special
103 events, including eclipse campaigns and geomagnetic storm monitoring periods.

104 The archival records consist primarily of 35 mm photographic film containing ionogram traces acquired by: C4 ionosonde
105 (1957–1994), IPS-42 system which delivered digital ionograms during an intermediate period (1999-2012), CADI for a few
106 days only, and IPS 42 after that. A substantial portion of this historical dataset had not been previously scaled and interpreted
107 or had undergone only partial manual scaling, representing a significant untapped scientific resource for long-term
108 ionospheric studies.

109 **2.3 Data Processing Pipeline**

110 *2.3.1 Digitization: SoCio Software*

111 Ionograms preserved on celluloid film were digitized using an Epson Perfection V600 Photo scanner at 1200 dpi resolution
112 to ensure adequate capture of trace details and frequency-height grid specifications. The digitized images required geometric
113 correction due to perspective distortion, film degradation, and variations in original recording formats across different
114 ionosonde systems.

115 To address these challenges, we developed the Software de Corrección de Ionogramas (*SoCio*; Urra, 2026), a MATLAB-
116 based tool specifically designed for geometric correction and standardization of historical ionogram imagery. *SoCio* applies
117 perspective correction algorithms to compensate for scanning distortions, and standardizes image dimensions according to
118 the specific ionosonde system that generated each record. The software includes modules for handling common film
119 deterioration artifacts, including opaque regions, physical damage, and inconsistent image density. This preprocessing step

120 was essential for ensuring accurate subsequent parameter extraction, as uncorrected geometric distortions can introduce
121 systematic errors in frequency and height measurements.

122 *2.3.2 Scaling: DISS Software Enhancement*

123 Following geometric correction, ionospheric parameters were extracted using the Digitized Ionogram Scaling Software
124 (DISS v. 3.0), previously employed in eclipse observation campaigns (Bravo et al., 2020). For the present study, DISS
125 capabilities were substantially enhanced to accommodate the diversity and technical challenges of the historical dataset. Key
126 improvements included: (1) implementation of interactive trace digitization tools enabling manual extraction of frequency-
127 virtual height coordinates from user-drawn traces on the ionogram display, (2) development of selectable region-of-interest
128 functionality to isolate specific ionospheric layers for detailed analysis, (3) incorporation of adjustable frequency and height
129 calibration parameters to fine-tune the pixel-to-physical-unit conversion for each ionogram variant, and (4) integration of
130 quality control modules to identify and flag problematic traces requiring manual review.

131 These enhancements enabled DISS to handle the heterogeneous characteristics of multi-decade ionosonde observations,
132 including variations in frequency sweep ranges (typically 1–20 MHz with system-dependent upper limits), height display
133 scales (100–500 km, later extended to 1000 km for topside observations), and trace characteristics influenced by film aging
134 and storage conditions.

135 *2.3.3 Parameter Extraction*

136 From each scaled ionogram, we extracted the following standard ionospheric parameters: critical frequencies of the E, F1,
137 and F2 layers (f_oE , f_oF1 , f_oF2) and their corresponding virtual heights ($h'E$, $h'F1$, $h'F/F2$), according the rules given by
138 Piggott & Rawer (1972).

139 **2.4 Statistical Analysis and Eclipse Response Quantification**

140 Eclipse-induced ionospheric perturbations were quantified by calculating both absolute and percentage deviations of critical
141 frequencies relative to reference day values at corresponding local times. Absolute deviations were computed as:

$$142 \quad \Delta f_oL = f_oL_{eclipse} - f_oL_{reference}$$

143 where L represents the ionospheric layer (E, F1, F2). Percentage deviations were calculated as:

$$144 \quad \% \Delta f_oL = \frac{f_oL_{eclipse} - f_oL_{reference}}{f_oL_{reference}} \times 100.$$

145 Reference day values were obtained from hourly monthly median parameters for each eclipse event, selecting the median
146 value across multiple reference days to minimize day-to-day ionospheric variability. These hourly monthly medians had

147 been previously scaled for the World Data Centre. When hourly monthly median values were unavailable, the previous day
148 was used as the reference condition (03-11-1994, 11-09-2007, 13-11-2012, 30-04-2022 and 02-10-2024 solar eclipses). In
149 two particular cases, neither the hourly monthly median values nor the previous day provided suitable reference conditions
150 during the eclipse interval. In these cases, the International Reference Ionosphere (IRI) 2020 model (Bilitza et al., 2022) was
151 used, specifically for foF1 during the 12-11-1966 solar eclipse and for foE during the 14-12-2020 solar eclipse.

152 When multiple measurements were available during the eclipse period (depending on the operational cadence: 1, 5, 15, 30,
153 or 60 minutes), we selected the observation closest to the time of maximum obscuration for regression analysis. Linear
154 regression analysis was performed using SciPy's linregress function from stats module (SciPy v1.17.1) to investigate the
155 functional relationship between solar obscuration percentage (independent variable, x) and ionospheric parameter deviations
156 (dependent variable, y). The regression model adopted was:

$$157 \quad y = mx + b$$

158 where m represents the sensitivity of the ionospheric parameter to eclipse magnitude (slope) and b the intercept. The
159 goodness of fit was assessed using the coefficient of determination (r^2), computed as:

$$160 \quad r^2 = 1 - \frac{\sum_{i=1}^n (y_i - \hat{y}_i)^2}{\sum_{i=1}^n (y_i - \bar{y})^2}$$

161 where y_i are observed values, \hat{y}_i are predicted values from the regression line, and \bar{y} is the mean of observed values. r^2
162 quantifies the proportion of variance in ionospheric response explained by solar obscuration, with values ranging from 0 (no
163 explanatory power) to 1 (perfect prediction). To evaluate the statistical significance of the regression, the p-value associated
164 with the slope of the model will be used, considering a significance level of $\alpha = 0.05$ to reject the null hypothesis of absence
165 of linear dependence.

166 From the initial catalog of 21 eclipse events identified over the period 1957–2024 (see Table 1), ionosonde records were
167 available for only 16 events (76%). Among these, we selected events exhibiting clear ionospheric signatures and sufficient
168 data coverage during the eclipse period. Both absolute (MHz) and percentage (%) deviations were analyzed to assess
169 whether normalization by baseline values improved the linearity of the response to the eclipse. The heterogeneous nature of
170 the dataset—comprising observations from three different ionosonde systems (C4, IPS-42, CADI) with varying temporal
171 resolutions—introduces additional variability that may affect correlation strength, particularly for parameters sensitive to
172 instrumental characteristics.

173 Using the established regression relationships, we computed predicted ionospheric responses for the upcoming 06 February
 174 2027 solar eclipse, during which Chillán is expected to experience approximately 70% solar obscuration (last row of Table
 175 1). These predictions are indicated by orange star markers in all regression plots, providing quantitative forecasts to support
 176 observation campaign planning.

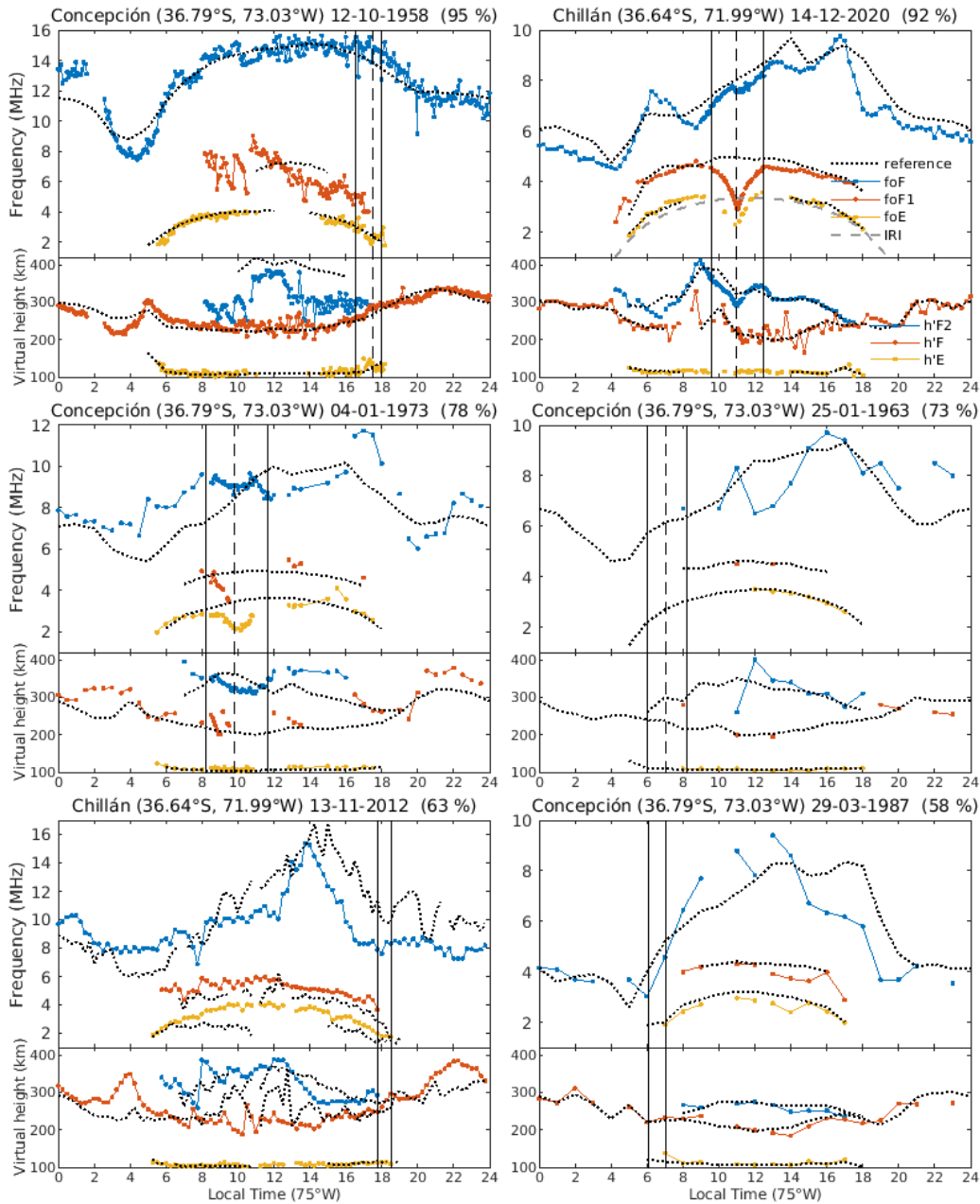
177 **Table 1:** Timing of selected solar eclipses over Concepción/Chillán (Maximum obscuration >15%) from 1958 to 2030, including start,
 178 maximum, and end times at ground level, according to Eclipse Calculator 2.0 (Masana, 2012). Local time (LT) corresponds to the 75°W
 179 meridian. Adjusted F10.7 solar flux values were obtained from the Space Weather Services at Collecte Localisation Satellites (CLS,
 180 <https://spaceweather.cls.fr/>).

#	Date (DD-MM-YYYY)	Start time in Concepción (hh:mm LT)	Maximum time in Concepción (hh:mm LT)	End time in Concepción (hh:mm LT)	Maximum obscuration in Concepción/Chillán (%)	Ionospheric Station: j3o, Concepción; j3p, Chillán	Eclipse-time sampling interval	Adjusted F10.7 Solar Flux (sfu)
1	12-10-1958	16:32	17:31	18:01	95	j3o: C4, cross deltas, 1-25 MHz	5 min film	219.3
2	25-01-1963	06:02	07:04	08:14	73	j3o: C4, cross deltas, 1-25 MHz	1 hour film	72.2
3	12-11-1966	07:46	08:51	10:00	49	j3o: C4, folded dipole + logperiodic, 0.25-20 MHz	5 min film	126.3
4	11-09-1969	16:03	16:53	17:35	20	j3o: C4, folded dipole + logperiodic, 0.25-20 MHz	30 min film	119.0
5	04-01-1973	08:14	09:50	11:39	78	j3o: C4, folded dipole + logperiodic, 0.25-20 MHz	5 min film	109.3
6	03-11-1975	06:22	07:06	07:52	19	j3o	Instrument failure	73.0
7	22-08-1979	11:35	13:04	14:27	31	j3o: C4, cross deltas, 0.25-20 MHz	30 min film	223.2
8	10-08-1980	14:47	15:51	16:49	27	j3o: C4, cross deltas, 0.25-20 MHz	No data	173.5
9	04-02-1981	17:25	18:18	18:56	43	j3o: C4, cross deltas, 0.25-20 MHz	1 hour film	197.5
10	12-11-1985	07:36	08:20	09:06	17	j3o: C4, cross deltas, 0.25-20 MHz	1 hour film	74.7
11	29-03-1987	06:07	06:07	07:01	58	j3o: C4, cross deltas, 0.25-20 MHz	1 hour film	75.3
12	26-01-1990	14:30	15:28	16:22	23	j3o: C4, cross deltas, 0.25-20 MHz	1 hour film	238.8

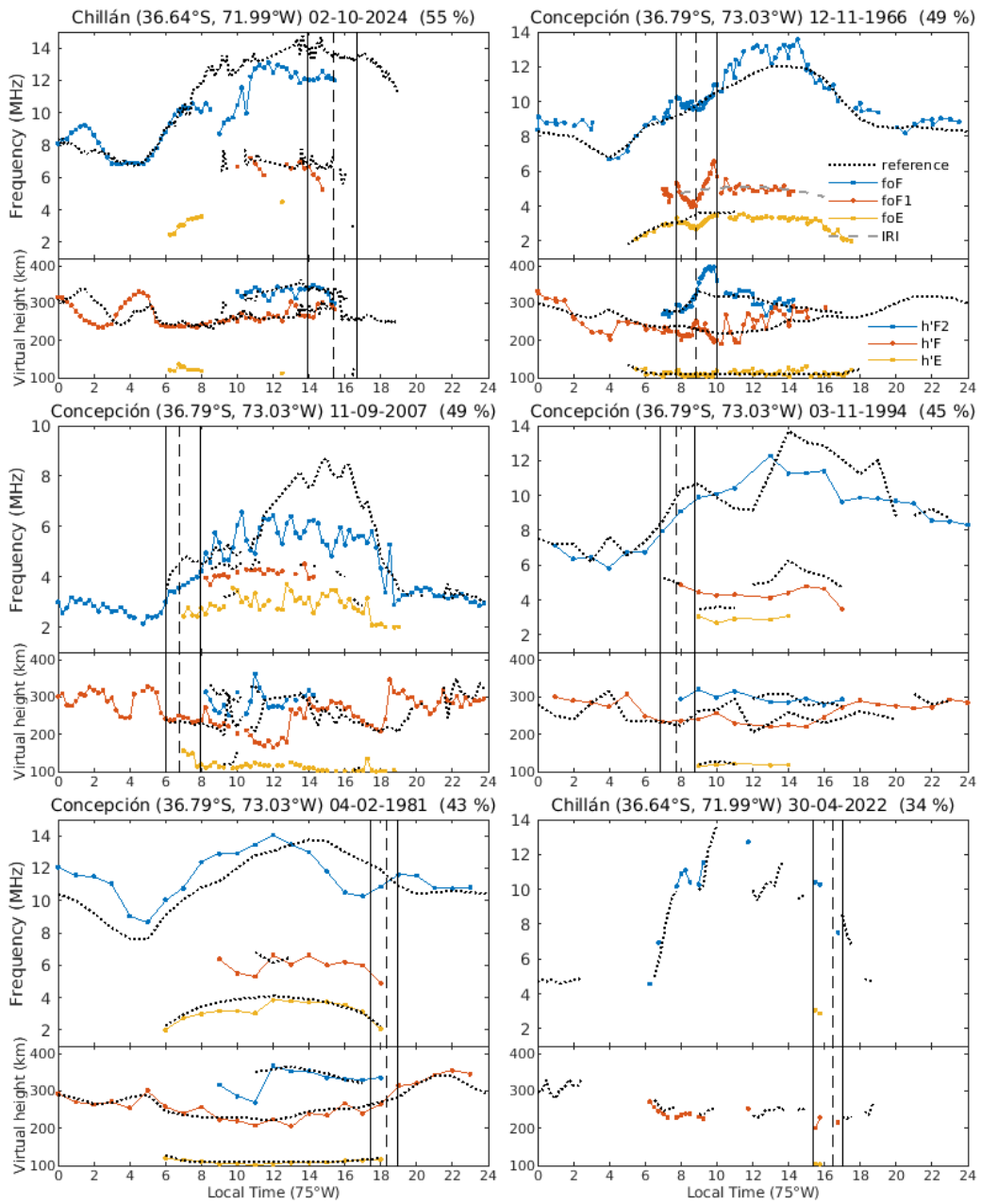
13	03-11-1994	06:49	07:45	08:46	45	j3o: C4, cross deltas, 0.25-20 MHz	1 hour film	85.9
14	11-09-2007	06:03	06:46	07:55	49	j3o: IPS 42, cross deltas, 1-22 MHz	15 min digital	67.0
15	11-07-2010	14:54	15:58	16:47	62	j3o: IPS 42, cross deltas, 1-22 MHz	No data	85.4
16	13-11-2012	17:48	18:34	18:34	63	j3p: IPS 42, cross deltas, 1-22 MHz	15 min digital	143.1
17	26-02-2017	07:18	08:30	09:51	67	j3p	Instrument failure	77.5
18	02-07-2019	14:16	15:31	16:38	81	j3p	Instrument failure	69.5
19	14-12-2020	09:36	11:00	12:28	92	j3p: IPS 42, cross deltas, 1-22 MHz	1 min digital	80.4
20	30-04-2022	15:21	16:30	17:03	34	j3p: IPS 42, cross deltas, 1-22 MHz	15 min digital	121.5
21	02-10-2024	13:56	15:24	16:42	55	j3p: IPS 42, cross deltas, 1-22 MHz	5 min digital	274.8
22	06-02-2027	08:21	09:56	11:39	70	-	-	-

181 **3 Results and Discussion**

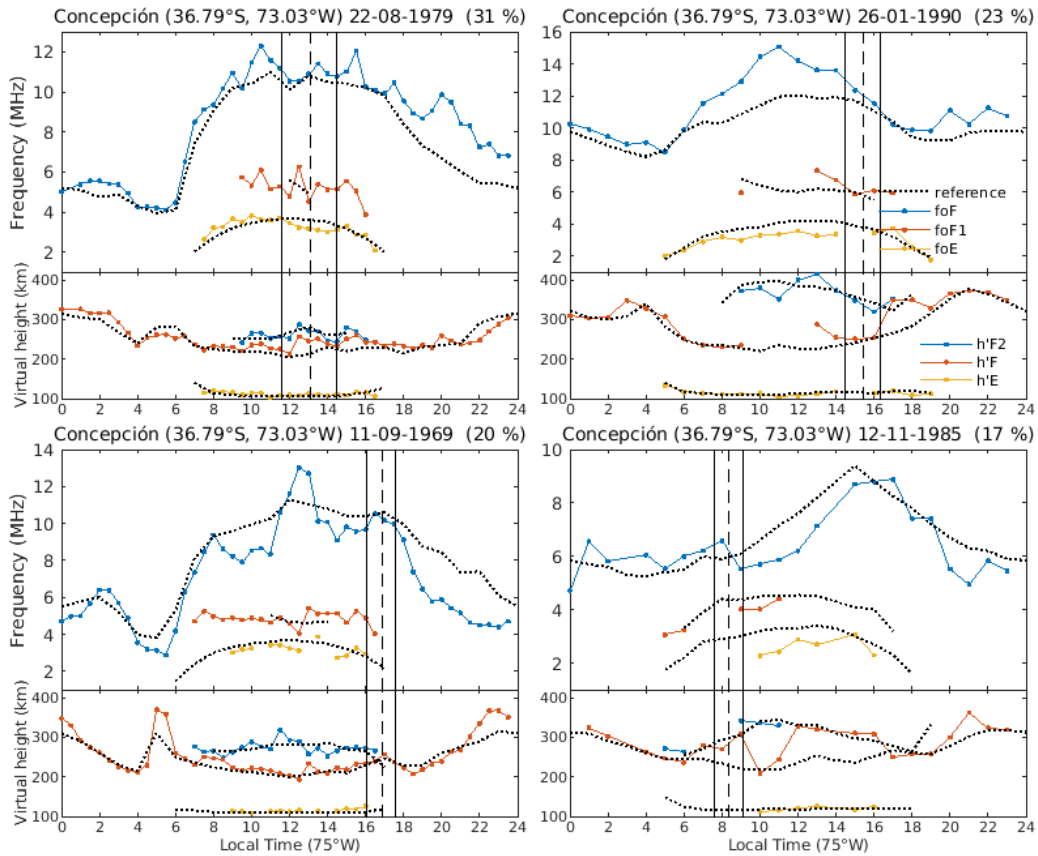
182 The diurnal variations of critical frequencies and virtual heights observed during the days in which the 16 selected eclipses
183 occur are shown in Figures 1 to 3. Reference curves are also shown for comparison. As already indicated, observed values
184 are given at different time intervals as appropriate to the available ionograms for the different eclipses. Diurnal variations are
185 arranged according to the obscuration level, regardless of the time-of-day, month, year or solar activity epoch.



186 **Figure 1:** Diurnal variation of observed critical frequencies and virtual height (dots) on days of various solar eclipses with obscuration
 187 levels greater than 55% and corresponding monthly median values (dotted line). Dates are given in DD-MM-YYYY format and the
 188 maximum obscuration percentage is indicated in parentheses. Continuous vertical lines indicate onset and end of eclipse. The slash vertical
 189 line indicates the time of maximum darkness. Note that for eclipses occurring near sunrise (sunset), the time of maximum obscuration may
 190 coincide with the beginning (end) of the partial solar eclipse.



192 **Figure 2:** As of Figure 1 but for obscuration level between 34 % and 55 %.



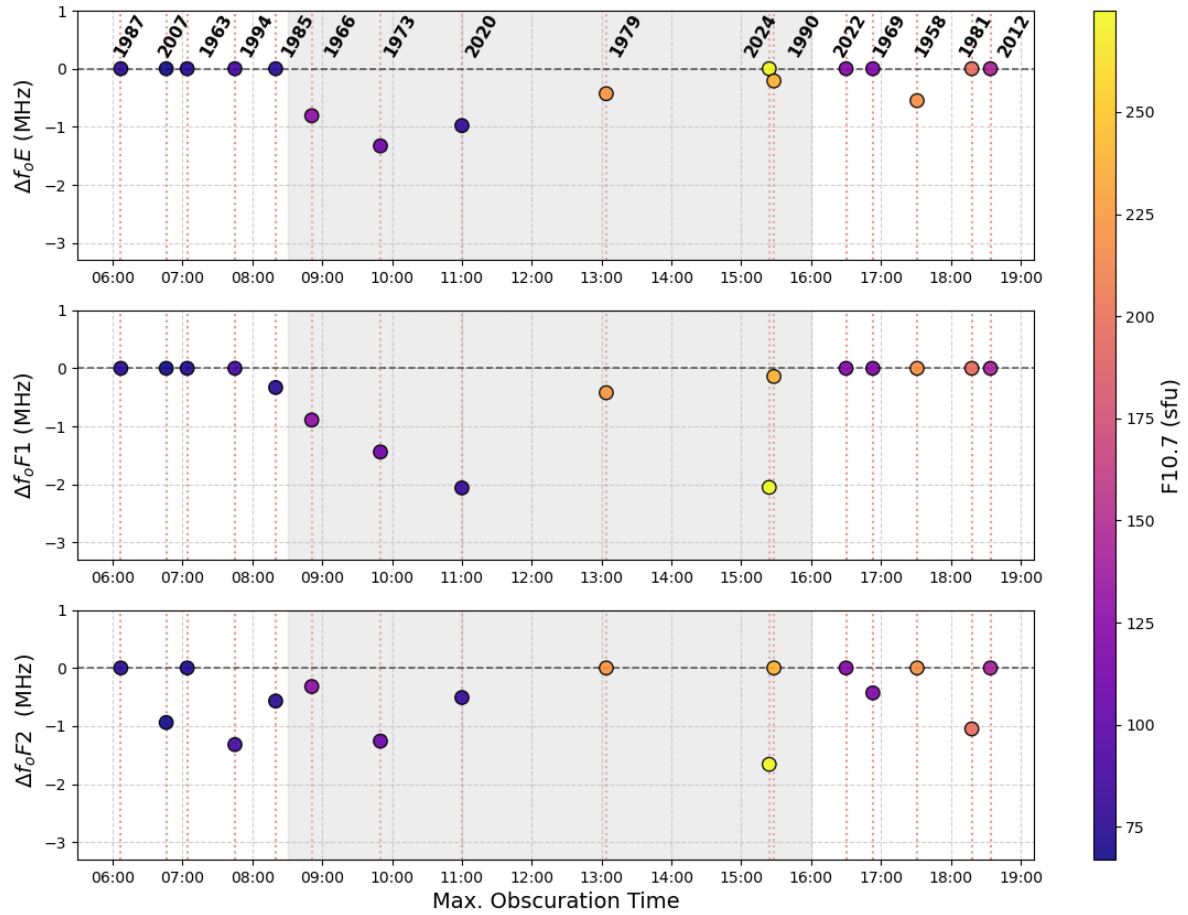
193 **Figure 3:** Same as Figure 1, but for obscuration level between 17 % and 31 %.

194 The clearer ionospheric effects of eclipses are seen, as expected, during eclipses occurring just before or around local noon.
 195 The maximum level of obscuration ranges from 31% to 92% for these eclipses, thus allowing to determine a fairly
 196 dependence of ionospheric effects on darkness level. The critical frequencies of the F1 and E layers show a typical dip
 197 variation, while the critical frequency of the F2 layer has more complex variations, probably showing two different stages,
 198 before and after the maximum darkness level, somehow following the variations of h'F/F2. The E layer virtual height does
 199 not seem to significantly change during these eclipses.

200 Figure 4 presents the foE, foF1, and foF2 deviations, calculated as the difference between the minimum value observed
 201 during the eclipse interval and the corresponding reference value. The adjusted F10.7 solar flux corresponding to each event
 202 is indicated by the color scale shown in the right-hand bar. Clearer variations can be identified for foE and foF1 during
 203 specific daytime intervals, whereas the foF2 response appears less well defined. To obtain the most suitable set of
 204 differences for the linear regression analysis, only eclipse events with maximum obscuration occurring between 08:30 and
 205 16:00 LT (75°W) were selected. These correspond to six events, listed in Table 2. When no differences are observed

206 between the reference curve and the day of the eclipse, or due to a lack of data or other reasons mentioned below, a zero
207 value is recorded for the frequency deviations

208



209 **Figure 4:** foE, foF1, and foF2 deviations at the time of maximum obscuration for the 16 selected events. The shaded (gray) area indicates
210 the time interval in which the selected events are found (08:30 -16:00 LT). Colors indicate the adjusted F10.7 solar flux.

211 These six selected events (29%) exhibited clear ionospheric signatures and sufficient data coverage during the eclipse period
212 for the regression analysis (Figure 5). The remaining 10 events (48%) were not considered due to one or more of the
213 following limitations: (1) missing observations during critical eclipse phases (particularly around maximum obscuration), (2)
214 eclipse occurrence near sunrise or sunset when ionospheric conditions are rapidly changing, making it difficult to isolate
215 eclipse effects from diurnal variations, (3) severe film degradation preventing reliable parameter extraction despite multiple
216 scaling attempts, or (4) obscuration levels below the detection threshold for significant ionospheric perturbations. It should
217 be noted that the regression analysis was performed only on critical frequencies and not on virtual heights. Changes in virtual
218 heights ($h'E$, $h'F1$, $h'F/F2$) were observed to be inconsistent—sometimes increasing, sometimes decreasing—making
219 prediction difficult. These variations are likely influenced by additional factors such as neutral winds, plasma transport, and
220 other dynamical processes, which complicate their response to eclipse conditions.

221

222 **Table 2:** Selected solar eclipses over Concepción/Chillán used for the linear regression analysis, including maximum obscuration at
223 ground level, according to Eclipse Calculator 2.0 (Masana, 2012). Local time (LT) corresponds to the 75°W meridian. Adjusted F10.7
224 solar flux values were obtained from the Space Weather Services at Collecte Localisation Satellites (CLS, <https://spaceweather.cls.fr/>).

225

Date (DD-MM-YYYY)	Maximum time (hh:mm LT)	Maximum obscuration (%)	Adjusted F10.7 Solar Flux (sfu)
12-11-1966	08:51	49	126.3
04-01-1973	09:50	78	109.3
22-08-1979	13:04	31	223.2
26-01-1990	15:28	23	238.8
14-12-2020	11:00	92	80.4
02-10-2024	15:24	55	274.8

226

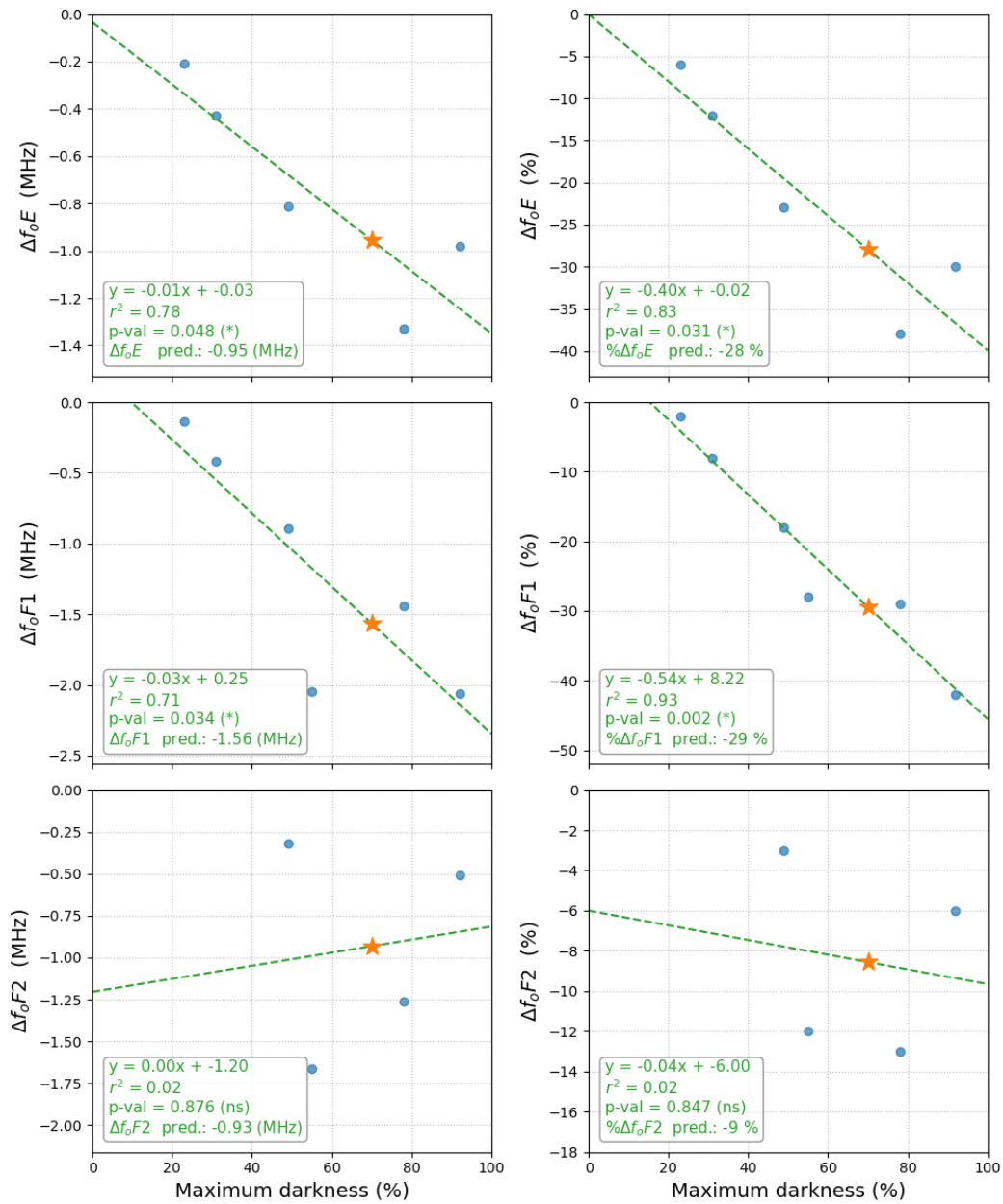
227

228

229

230

231



233 **Figure 5:** Linear regression analysis of ionospheric parameter deviations versus solar obscuration percentage during six eclipse events
 234 (1957–2024, blue circles). Left column: absolute frequency deviations (MHz). Right column: percentage deviations (%). Green dashed
 235 lines represent least-squares linear fits with equations, r^2 , p-value and predicted values shown. Orange stars indicate predicted responses
 236 for the 06 February 2027 eclipse (70% obscuration at Chillán).

237 Analyzing Figure 5, the E-layer critical frequency (foE) exhibited a robust linear response to solar obscuration, with absolute
238 deviations showing the strongest correlation among all analyzed parameters ($r^2 = 0.78$, $n = 5$ events, upper left panel). The
239 regression yielded a slope -0.01 of MHz per percent obscuration and an intercept of -0.03 MHz, indicating that foE decreases
240 nearly proportionally to eclipse magnitude. This relationship implies that a hypothetical total eclipse (100% obscuration)
241 would reduce foE by approximately 1.0 MHz relative to unperturbed reference conditions. The p -value = 0.05 is in the limit
242 of the conventional significance threshold ($\alpha = 0.05$), indicating that the relationship is statistically significant (*). In relative
243 terms (%), the relationship is even stronger ($r^2 = 0.83$, $p = 0.03$).

244 The high proportion of explained variance ($r^2 = 0.78$) reflects the rapid photochemical equilibrium characteristic of the E-
245 region, where recombination timescales (20-40 minutes) are comparable to or shorter than typical eclipse durations.
246 Consequently, E-layer ionization density responds almost instantaneously to variations in solar EUV flux, with minimal
247 influence from dynamic processes such as neutral winds or plasma diffusion that complicate interpretation of higher-altitude
248 layers.

249 When analysing foF1 response, in MHz values, the fit is linearly significant ($r^2 = 0.71$, $p = 0.034$), demonstrating a direct
250 dependence on solar obscuration. However, when normalizing the data as a percentage (%), the linear relationship becomes
251 outstanding and exhibits the most robust coupling in the entire study ($r^2 = 0.93$, $p = 0.002$). This remarkable improvement
252 when using relative values suggests that normalization successfully eliminates the variability of the baseline (seasonal and
253 solar cycle) conditions for each eclipse, revealing that the behavior of the F1 layer is governed almost purely by
254 photochemical control proportional to the radiation loss.

255 Regarding the response of the F2 layer, there is no evidence of a linear dependence on the darkening. The r^2 values are
256 practically zero (0.02) and the p values are extremely high (0.88 and 0.85). This leads to accepting (not rejecting) the null
257 hypothesis: the variation of ΔfoF2 during the analyzed eclipses appears to be dominated by external dynamic factors, such as
258 thermospheric winds or plasma transport, rather than by instantaneous local photoionization.

259 An additional source of complexity in the observed ionospheric response arises from the varying trajectories of the analyzed
260 solar eclipses. Specifically, eclipse paths that intersect the Equatorial Ionization Anomaly (EIA) region can significantly alter
261 regional electrodynamics rather than just local photochemistry. Obscuration over low latitudes reduces the E-region
262 conductivity, which subsequently weakens the equatorial $\mathbf{E} \times \mathbf{B}$ vertical drift and modulates the equatorial fountain effect
263 (e.g., Bravo et al, 2020). Consequently, this disruption in the poleward plasma transport introduces further variability in the
264 observed foF2 measurements over mid-latitude stations like Concepción/Chillán. For such events, the ionospheric depletion
265 is a complex superimposition of local photochemical loss and altered remote dynamical transport, which may explain the
266 high dispersion observed in the F2-layer data points across different eclipses.

267 Based on the established relationship, the 06 February 2027 eclipse (70% obscuration at Chillán) is predicted to induce a foE
268 reduction of 0.95 MHz (orange star, Figure 5, upper left panel). This forecast will enable direct validation of the regression
269 model and assessment of its predictive skill.

270 Several campaigns were conducted historically to obtain ionograms at higher temporal resolution during eclipses, with
271 observations every 5 minutes for significant events. However, most of these high-cadence data were never published. We
272 noted that cases with higher temporal resolution provided a significantly clearer depiction of the ionospheric response to the
273 lunar shadow, whereas 1-hour cadence datasets typically captured only one or two measurements during the obscuration
274 period. This difference in temporal resolution may affect the regression analysis, as the exact moment of maximum
275 obscuration is not always captured by the low-cadence measurements.

276 For the 2 July 2019 solar eclipse, there was a unique opportunity to measure the ionospheric response at two locations in
277 Chile: Chillán (36.64°S, 71.99°W) and La Serena (29.9°S, 71.3°W). However, the ionosonde in Chillán failed during the
278 event, so only the response at La Serena was published (Bravo et al., 2020). One of the analyzed events corresponds to the
279 14 December 2020 solar eclipse over Chillán, for which ionospheric responses were also studied by de Haro Barbas et al.
280 (2022). Their results included calculations of the alpha and beta recombination coefficients, which were found to be
281 consistent with values reported by previous authors, confirming the reliability of the ionospheric observations in this region.
282 Furthermore, prior to the 2020 eclipse, a prediction of the ionospheric response over the Chillán station had been performed
283 using the SUPIM-INPE model, estimating the expected variations in the different ionospheric layers during the event
284 (Martínez-Ledesma et al., 2020). This prediction was later validated using the observed ionospheric data, as reported in
285 Bravo et al. (2022), showing good agreement between the modeled and measured responses.

286 It is important to highlight the dedicated effort of ionosonde operators and technicians, particularly during the 1958–1994
287 period, who ensured continuous monitoring and undertook the considerable effort of recording frequent ionograms during
288 eclipses. Recovering historical data from analog ionograms stored unprocessed for decades presents a significant
289 methodological and technical challenge. The first obstacle lies in the state of preservation of the physical medium (typically
290 film reels), whose natural degradation necessitates an extremely rigorous scanning process to preserve information and
291 capture optimal contrast without damaging the medium. Subsequently, the workflow requires digital clipping to extract and
292 isolate each ionogram from the continuous record, a task that involves meticulously correcting optical and non-linear
293 distortions along the frequency and virtual height axes. Finally, parameter extraction is extremely complex: although scaling
294 systems (such as DISS software) are used, internal imperfections in the old recording – such as high background noise,
295 physical rays on the film, and diffuse traces – severely limit the effectiveness of modern pattern recognition algorithms.
296 Consequently, the software often requires constant and thorough manual intervention by an expert operator to validate,
297 correct, or redraw the traces, making the recovery of these time series a highly labor-intensive task.

298 The present study relied on a historical dataset that represents a significant rescue of scientific heritage. Many records were
299 on obsolete 35 mm film, degraded, or even potentially flammable, and have now been digitized and standardized for
300 analysis. Similar conditions exist at other older ionospheric stations, emphasizing the importance of preserving long-term
301 ionospheric observations and fully exploiting their scientific value.

302 **4 Conclusion**

303 This work analyzed the response of the Concepción/Chillán ionosphere to six selected solar eclipses, out of a total of 21
304 identified events (29%) over the period 1958–2024, using a long-term historical ionogram dataset. Critical frequencies and
305 virtual heights were extracted from scaled ionograms, and regression analysis was performed to quantify the relationship
306 between solar obscuration and ionospheric parameter deviations. The study demonstrates that the E and F1 layers respond
307 nearly linearly to eclipse-induced reductions in solar radiation, while higher layers, particularly the F2 layer, exhibit more
308 complex and variable behavior due to additional dynamical processes. High-resolution observations, when available,
309 provided insights into short-term responses and enabled predictions for future eclipses.

310 Regression analysis focused exclusively on critical frequencies, as virtual heights often exhibited inconsistent behavior,
311 reflecting the influence of neutral winds, plasma transport, and other dynamical factors that complicate their interpretation. It
312 is important to note that only the ionospheric responses measured at Chillán during the 2 July 2019 and 14 December 2020
313 eclipses were published; no data from the remaining eclipse events have been published. The success of this study relied
314 heavily on the dedication of ionosonde operators and technicians, particularly during the 1958–1994 period, who ensured
315 frequent and reliable observations during solar eclipses. Moreover, this work represents a significant rescue of scientific
316 heritage, digitizing and standardizing records that were previously on fragile or potentially hazardous 35 mm film.
317 Recovering decades-old analog ionogram data presents major technical challenges across three stages: (1) carefully scanning
318 fragile, degrading film reels; (2) digitally clipping and correcting non-linear distortions on the axes; and (3) scaling the
319 parameters, where heavy background noise and film damage severely limit semi-automatic software (like DISS), requiring
320 constant, labor-intensive manual corrections by experts. Preserving and exploiting these long-term datasets is crucial for
321 advancing the understanding of ionospheric dynamics.

322 Predictions for the upcoming 06 February 2027 eclipse, with an expected 70% obscuration at Chillán, indicate a foE and
323 foF1 decrease of 0.95 MHz ($\% \Delta \text{foE} = 28\%$) and 1.56 MHz ($\% \Delta \text{foF1} = 29\%$), respectively, providing a clear opportunity to
324 validate the regression models and assess their predictive skill across different solar cycle conditions.

325 **Data availability**

326 Adjusted F10.7 solar flux values were obtained from the Space Weather Services at Collecte Localisation Satellites (CLS,
327 <https://spaceweather.cls.fr/>). The *SoCio* code is available at <https://github.com/BenjaUP-coding/SoCio>. The *Eclipse*
328 *Calculator 2.0* application (Masana, 2012) can be found at <https://serviastro.ub.edu/en/materials/apps/eclipsi-20>. Historical
329 scaled ionospheric data during solar eclipse events are currently available at <https://11nk.dev/hklvhci>.

330

331 **Author contributions**

332 AYG: writing (original draft preparation) and data curation; MAB: Conceptualization, writing (original draft preparation)
333 and formal analysis; CAC-R: data curation; MRC: data curation; BAU: methodology and data curation; AJF: supervision
334 and validation.

335

336 **Competing interests**

337 Manuel Bravo is the guest editor of the special issue.

338

339 **Acknowledgements**

340 We are indebted to the engineers and technicians who operated the C4 and IPSS-42 ionosondes from 1957 onwards; without
341 their work, this report would not have been possible. In particular, we thank Carlos Figueroa, Herwing Herrera, José Rivera,
342 Avelino Sáez, and others. This work was supported by the Universidad Adventista de Chile, regular projects PI-175 and PI-
343 204. MAB and BAU acknowledge the ANID/SUBDIRECCIÓN DE INVESTIGACIÓN APLICADA ID25I10556. MAB
344 also acknowledge the ANID/FONDECYT Iniciación 11261653. The authors acknowledge the assistance of Sider.ai in the
345 translation and preliminary review of the manuscript draft, with the subsequent and exhaustive manual scientific validation.

346 **References**

- 347 Afraimovich, E. L., Kosogorov, E. A., & Lesyuta, O. S.: Effects of the August 11, 1999 total solar eclipse as deduced from
348 total electron content measurements at the GPS network. *Journal of Atmospheric and Solar-Terrestrial Physics*,
349 64(18), 1933–1941, doi:10.1016/s1364-6826(02)00221-3, 2022.
- 350 Aryal, S., Geddes, G., Fin, S. C., Mrak, S., Galkin, I., Cnossen, I., et al.: Multi-spectral and multi instrument observation of
351 TIDs following the Total Solar Eclipse of August 21. *Journal of Geophysical Research: Space Physics*, 124, 3761–
352 3774, doi:10.1029/2018JA026333, 2019.
- 353 Bilitza, D., Pezzopane, M., Truhlik, V., Altadill, D., Reinisch, B. W., & Pignalberi, A.: The International Reference
354 Ionosphere model: A review and description of an ionospheric benchmark. *Reviews of Geophysics*, 60,
355 e2022RG000792. doi:10.1029/2022RG000792, 2022.

- 356 Bravo, M. A., Foppiano, A. J., and Abarca del Río, R.: Long-Term Dependencies of Annual and Semiannual Components of
357 NmF2 Over Concepción. *The Open Atmospheric Science Journal*, 5(1), 2-8, doi:10.2174/1874282301105010002,
358 2011.
- 359 Bravo, M., Martínez-Ledesma, M., Foppiano, A., Urra, B., Ovalle, E., Villalobos, C., Souza, J., Carrasco, E., Muñoz, P.,
360 Tamblay, L., Vega-Jorquera, P., Marín, J., Pacheco, R., Rojo, E., Leiva, R. & Stepanova, M.: First report of an eclipse
361 from Chilean ionosonde observations: comparison with total electron content estimations and the modeled maximum
362 electron concentration and its height. *J. Geophys. Res. Space Physics*, 125, e2020JA027923.
363 doi:10.1029/2020JA027923, 2020.
- 364 Bravo M.A., Molina M.G., Martínez-Ledesma M., de Haro Barbás B., Urra B., Elías A., Souza J., Villalobos C., Namour
365 J.H., Ovalle E., Venchiarutti J.V., Blunier S., Valdés-Abreu J.C., Guillermo E., Rojo E., de Pasquale L., Carrasco E.,
366 Leiva R., Castillo Rivera C., Foppiano A., Milla M., Muñoz P.R., Stepanova M., Valdivia J.A. and Cabrera M.:
367 Ionospheric response modeling under eclipse conditions: Evaluation of 14 December 2020, total solar eclipse
368 prediction over the South American sector. *Front. Astron Space Sci*, 9, doi: 10.3389/fspas.2022.1021910, 2022.
- 369 Bremer, J.: Ionospheric trends in mid-latitudes as a possible indicator of the atmospheric greenhouse effect, *Journal of*
370 *Atmospheric and Terrestrial Physics* 54, 1505-1511, 1992.
- 371 Cheng, K. H., Huang, Y. N., & Chen, S. W.: Ionospheric effects of the solar eclipse of September 23, 1987, around the
372 equatorial anomaly crest region. *Journal of Geophysical Research*, 97(A1), 103–111, doi:10.1029/91JA02409, 1992.
- 373 Chuo, Y. J.: Ionospheric effects on the F region during the sunrise for the annular solar eclipse over Taiwan on 21 May 2012,
374 *Ann. Geophys.*, 31, 1891–1898, doi:10.5194/angeo-31-1891-2013, 2013.
- 375 de Haro Barbás, BF, Bravo, M, Elias, AG, Martínez-Ledesma, M, Molina, G, Urra, B, Venchiarutti, JV, Villalobos, C,
376 Namour, JH, Ovalle, E, Guillermo, ED, Carrasco, E, de Pasquale, G, Rojo, E, Leiva R. Longitudinal variations of
377 ionospheric parameters near totality during the eclipse of December 14, 2020. *Adv. Space Res.*,
378 doi:10.1016/j.asr.2021.12.026, 2022.
- 379 Evans, J. V.: An F-region eclipse. *Journal of Geophysical Research*, 70(1), 131–142, doi: 10.1029/JZ070i001p00131, 1965a.
- 380 Evans, J. V.: On the behavior of foF2 during solar eclipses. *Journal of Geophysical Research*, 70(3), 733–738,
381 doi:10.1029/JZ070i003p00733, 1965b.
- 382 Foppiano, A.J.; Cid, L. and Jara, V.: Ionospheric long-term trends in South American mid-latitudes, *Journal of Atmospheric*
383 *and Solar-Terrestrial Physics*, 61, 717-723, 1999.
- 384 Higgs, A. J.: Ionospheric measurements made during the total solar eclipse of 1940 October 1. *Monthly Notices of the Royal*
385 *Astronomical Society*, 102(1), 24–34, doi:10.1093/mnras/102.1.24, 1942.
- 386 Hoque M.M., Wenzel, D., Jakowski, N., Gerzen, T., Berdermann, J., et al.: Ionospheric response over Europe during the
387 solar eclipse of March 20, 2015. *J. Space Weather Space Clim.*, 6, A36, doi:10.1051/swsc/2016032, 2016.
- 388 Huba, J. D., & Drob, D.: SAMI3 prediction of the impact of the 21 August 2017 total solar eclipse on the
389 ionosphere/plasmasphere system. *Geophysical Research Letters*, 44, 5928–5935. doi:0.1002/2017GL073549, 2017.

390 Jakowski, N., Stankov, S. M., Wilken, V., Borries, C., Altadill, D., Chum, J., et al.: Ionospheric behavior over Europe during
391 the solar eclipse of 3 October 2005. *Journal of Atmospheric and Solar-Terrestrial Physics*, 70(6), 836–853,
392 doi:10.1016/j.jastp.2007.02.016, 2008.

393 Jarvis, M.J., Jenkins, B., Rodgers, G.A.: Southern hemisphere observations of long-term decrease in F-region altitude and
394 thermospheric wind providing possible evidence for global thermospheric cooling, *Journal of Geophysical Research*,
395 103, 20774-20787, 1998.

396 Kumar, S., Singh, A. K., & Singh, R. P.: Ionospheric response to total solar eclipse of 22 July 2009 in different Indian
397 regions. *Annales de Geophysique*, 31(9), 1549–1558, doi:10.5194/angeo-31-1549-2013, 2013.

398 Lastovicka, J.: Progress in investigating long-term trends in the mesosphere, thermosphere, and ionosphere, *Atmos. Chem.*
399 *Phys.*, 23, 5783–5800, doi:10.5194/acp-23-5783-2023, 2023.

400 Laštovicka, J., Solomon, S.C. and Qian, L.: Trends in the Neutral and Ionized Upper Atmosphere, *Space Sci Rev*,
401 doi:10.1007/s11214-011-9799-3, 2017.

402 Le, H., Liu, L., Yue, X., and Wan, W.: The ionospheric responses to the 11 August 1999 solar eclipse: observations and
403 modeling, *Ann. Geophys.*, 26, 107–116, doi:10.5194/angeo-26-107-2008, 2008.

404 Le, H., Liu, L., Yue, X., Wan, W., and Ning B.: Latitudinal dependence of the ionospheric response to solar eclipses, *J.*
405 *Geophys. Res.*, 114, A07308, doi:10.1029/2009JA014072, 2009.

406 Lei, J., Dang, T., Wang, W., Burns, A., Zhang, B., & Le, H.: Long-lasting response of the global thermosphere and
407 ionosphere to the 21 August 2017 solar eclipse. *Journal of Geophysical Research: Space Physics*, 123, 4309–4316,
408 doi:10.1029/2018JA025460, 2018.

409 Martínez-Ledesma, M., Bravo, M., Urra, B., Souza, J., and Foppiano, A.: Prediction of the ionospheric response to the 14
410 December 2020 total solar eclipse using SUPIM-INPE. *JGR. Space Phys.* 125, e2020JA028625.
411 doi:10.1029/2020JA028625, 2020.

412 Masana, E.: Eclipsi 2.0 (Eclipse Calculator 2.0) [Mobile application software]. ServiAstro — Universitat de Barcelona.
413 Available in: <https://serviastro.ub.edu/en/materials/apps/eclipsi-20>, 2012.

414 Mitra, S. K., Rakshit, H., Syam, P., & Ghose, B. N.: Effect of the solar eclipse on the ionosphere. *Nature*, 132(3333), 442–
415 443. doi:10.1038/132442a0, 1933.

416 Momani, M. A., Yatim, B., & Mohd Ali, M. A.: Ionospheric and geomagnetic response to the total solar eclipse on 1 August
417 2008 over Northern Hemisphere. *Journal of Geophysical Research*, 115, A08321, doi:10.1029/2009JA014999, 2010.

418 Muzzioli, L.: La Estación de la Ionósfera, *Atenea No. 435*, 1er Semestre, 179-191, 1977.

419 Ortiz de Adler, N., Elías, A.G., Manzano, J.R.: Solar cycle length variations: its relation with ionospheric parameters.
420 *Journal of Atmospheric and Terrestrial Physics* 59, 159-162, 1997.

421 Ovalle E. M., Villalobos C. U., Agüero L. A., Leiva R. E., Foppiano A. J.: A new ionospheric station for Chile, *Bulletin No*
422 *74*, Ionospheric Network Advisory Group, Union Radio Scientific Internationale, 2017.

423 Pezzopane, M., Pietrella, M., Pignalberi, A., & Tozzia, R.: 20 March 2015 solar eclipse influence on sporadic E layer.
424 Advances in Space Research, 56(10), 2064–2072, doi:10.1016/j.asr.2015.08.001, 2015.

425 Piggott, W. R. & Rawer, K.: U.R.S.I. Handbook of Ionogram Interpretation and Reduction. U.S. Department of Commerce
426 National Oceanic and Atmospheric Administration-Environmental Data Service, Asheville, North Carolina, USA,
427 326 pp., 1972.

428 Ramírez, P.M.: Física de la ionósfera e interpretación de los ionogramas obtenidos en la Estación Concepción, como
429 colaboración al Año Geofísico Internacional, Facultad de Ingeniería, Universidad de Concepción, 1963.

430 Ratcliffe, J. A.: A survey of solar eclipses and the ionosphere. In W. J. G. Beynon & G. M. Brown (Eds.), Solar eclipses and
431 the ionosphere (pp. 1–13). Oxford: Pergamon Press, 1956.

432 Reinisch, B. W., Dandenault, P. B., Galkin, I. A., Hamel, R., & Richards, P. G.: Investigation of the electron density
433 variation during the 21 August 2017 solar eclipse. Geophysical Research Letters, 45, 1253–1261, doi:
434 10.1002/2017GL076572, 2018.

435 Rishbeth, H.: Solar eclipses and ionospheric theory. Space Science Reviews, 8(4), 543–554. doi:10.1007/BF00175006, 1968.

436 Smith, P.A., King, J.W.: Long-term relationships between sunspots, solar faculae and the ionosphere. Journal of
437 Atmospheric and Terrestrial Physics 43, 1057-1063, 1981.

438 Urra, B.: SoCIo, Software de Corrección de Ionogramas , <https://github.com/BenjaUP-coding/SoCIo>, 2026.

439 Zhang, H., Zhang, T., Zhang, X., Yuan, Y., Wang, Y., & Ma, Y.: Multi-Instrument Observations of the Ionospheric
440 Response Caused by the 8 April 2024 Total Solar Eclipse. Remote Sensing, 16(13), 2451, doi:10.3390/rs16132451,
441 2024.